AIAA JOURNAL
Vol. 33, No. 4, April 1995

Stability of a Compressible Axisymmetric Swirling Jet

Mehdi R. Khorrami*
High Technology Corporation, Hampton, Virginia 23666

Temporal linear stability of a compressible swirling axisymmetric jet is considered. It is found that with the addition of a modest amount of swirl, instability growth rates are substantially increased. Additionally, rotating jets are found to be highly unstable for disturbances with high azimuthal wave numbers. Such disturbances are absent for the case of nonswirling jets. Most importantly, it is found that the stabilizing influence of increasing Mach number is diminished with the introduction of swirl to the jet flow.

Nomenclature

a_0 = centerline speed of sound
C_1 = constant
F = eigenfunction associated with disturbance radial velocity
G = eigenfunction associated with disturbance azimuthal velocity
H = eigenfunction associated with disturbance axial velocity
K = constant, a measure of axial momentum flux
M = Mach number, W_0/a_0
N = number of Chebyshev polynomials
n = azimuthal wave number
P = pressure eigenfunction
Pr = Prandtl number
$\tilde{p}$ = pressure
q = swirl ratio, ratio of maximum azimuthal velocity to maximum axial velocity
Re = Reynolds number, $\rho_0 W_0 r_0/\mu$
r = radial coordinate
r_c = critical layer position
r_0 = characteristic length scale
T = temperature eigenfunction
$\tilde{T}$ = temperature
t = time
U = mean radial velocity
V = mean azimuthal velocity
v_r, v_θ, v_z = three components of velocity in cylindrical coordinates
W = mean axial velocity
W_0 = maximum mean axial velocity
$\mathbf{y}$ = eigenfunction vector
z = axial coordinate
z_0 = some reference axial location
α = axial wave number
β = ratio of farfield temperature to centerline temperature
Γ = circulation
γ = ratio of specific heats
δ = density eigenfunction
η = mean temperature
η_0 = centerline temperature
η_∞ = farfield temperature
θ = azimuthal coordinate
κ = thermal conductivity
λ = bulk coefficient of viscosity
μ = dynamic viscosity
ν = kinematic viscosity
Π = mean pressure
ρ = mean density
$\tilde{\rho}$ = density
ρ_0 = centerline density
σ = constant related to the swirl ratio as defined in Eq. (11)
ϕ_0 = jet-spreading angle
ω = perturbation complex angular frequency
ω_i = imaginary part of frequency or perturbation growth rate
ω_r = real part of frequency

Presented as Paper 91-1770 at the AIAA 22nd Fluid Dynamics, Plasmadynamics, and Lasers Conference, Honolulu, HI, June 24–27, 1991; received Nov. 17, 1993; revision received May 24, 1994; accepted for publication May 31, 1994.

*Scientist, P.O. Box 7262. Senior Member AIAA.

I. Introduction

EFFICIENTmixing of air and fuel at high speeds is one of the central issues in designing supersonic combustion chambers. Inherent in these combustors are free shear layers which form as fuel is injected into the freestream. However, mixing in these shear layers is hampered because of the short residence time of flow molecules, due to the finite length of the chamber and the high flow speeds involved. Furthermore, it is well known that the growth rate of a shear layer is reduced substantially as Mach number increases.[1,2] Thus, the goal of much current supersonic combustion research is to enhance fuel/air mixing by altering shear-layer spreading rates in someway. A common strategy is to employ streamwise vortices or swirl.

Recently, in a series of experiments conducted at NASA Langley Research Center, Northam[3] and co-workers found that the addition of modest amounts of swirl to a generic combustor flowfield increased the entrainment rate of shear layers. Similarly, Taghavi et al.[4] found that both excited and unexcited swirling turbulent jets (at low subsonic Mach numbers) have higher spreading rates than a swirl-free jet. The few experiments available suggest that addition of swirl may significantly alter the underlying dynamics and developments of free shear layers. However, stability analysis for compressible swirling flows is lacking. Such analysis is needed to confirm the trends observed by experimenters and to identify some of the fundamental underlying physical mechanisms involved in these flows. Better understanding of the stability characteristics of compressible mixing layer is essential for optimizing control techniques. Therefore, as a model flow, the stability of a compressible swirling jet is considered.

Although the stability of axisymmetric compressible jets has received much attention in the past,[5] analyses for the rotating jet are almost nonexistent. To the author's knowledge, the recent paper of Coleman[6] is the only work on this subject. By superposing a Rankine vortex on a top-hat jet velocity field, Coleman analyzed the stability of the combined flow in the context of astrophysical phenomena. He found, for a wide range of Mach numbers, that the addition of swirl stabilizes the asymmetric instability modes with positive azimuthal wave number n and greatly reduces the growth rate of both the axisymmetric modes and the asymmetric modes with negative n. This stabilizing influence of rotation predicted by his analysis contradicts the experimentally observed trend. However, the mean flowfield employed by Coleman is neither a true vortex nor does it represent a

swirling jet accurately. Therefore, it is very difficult to compare his results with experiments or to draw any general conclusions. Consequently, a more detailed study with a more realistic flowfield is needed to understand the stability characteristics of compressible swirling jets.

The objectives of the present study are to understand the effects of rotation on the stability characteristics of a compressible jet and to explore the influence of compressibility (due to Mach number) on the stability of swirling flows. The analysis presented here is restricted to small rates of swirl relative to the jet velocity, which is appropriate for supersonic combustion chambers in which one must obtain the maximum amount of thrust from the fuel injectors. (High rotational speeds require energy expenditure without contributing additional thrust, whereas modest rates of swirl can be used to enhance mixing without significantly additional expenditure of energy.)

II. Formulation of the Stability Problem

In this section the linearized governing equations for variable property flows are derived. The equations are written for an arbitrary parallel mean flow. The waveform of the superposed disturbances as well as the numerical scheme employed to perform the temporal linear stability analysis are given. In the following section the parallel mean flowfield for a compressible swirling jet is outlined.

Cylindrical polar coordinates (r, θ, z) are employed. In this coordinate system, v_r, v_θ, v_z, $\tilde{p}$, $\tilde{T}$, and $\tilde{\rho}$ represent the three components of velocity, pressure, temperature, and density, respectively. Each flow variable is assumed to consist of a mean part and infinitesimally small perturbations. Utilizing normal-mode analysis, the perturbations are Fourier decomposed. The flow variables then are written

$$\begin{Bmatrix} v_r \\ v_\theta \\ v_z \\ \tilde{p} \\ \tilde{T} \\ \tilde{\rho} \end{Bmatrix} = \begin{Bmatrix} U(r) \\ V(r) \\ W(r) \\ \Pi(r) \\ \eta(r) \\ \rho(r) \end{Bmatrix} + \begin{Bmatrix} F(r) \\ G(r) \\ H(r) \\ P(r) \\ T(r) \\ \delta(r) \end{Bmatrix} e^{i(\alpha z + n\theta - \omega t)} \tag{1}$$

where α and n are the axial and azimuthal wave numbers, respectively, and ω the angular frequency. Substituting Eq. (1) into the Navier–Stokes equations for variable properties flow and neglecting second-order terms in the perturbations, the linearized governing equations in terms of the perturbation eigenfunctions are obtained. For a parallel flow, these equations are given in the Appendix. Note that the equation of state for an ideal gas was used to eliminate density perturbations. Furthermore, perturbations in the flow properties are related to temperature perturbations via the assumed functional form of viscosity and thermal conductivity.

The governing equations, presented in a laboratory frame of reference, are normalized with respect to the jet centerline values and a characteristic length scale r_0 to be defined later.

For a well-posed problem, the set of governing equations needs eight boundary conditions. At the far-field boundary, the disturbances are forced to approach zero. That is,

$$F(\infty) = G(\infty) = H(\infty) = T(\infty) = 0 \tag{2}$$

as $r \to \infty$. The conditions on the centerline are dependent on the azimuthal wave number. For single valued and smooth solutions, the following boundary conditions are required at $r = 0$:

If $n = 0$,

$$\begin{aligned} F(0) &= G(0) = 0 \\ \frac{dH}{dr}(0) &= \frac{dT}{dr}(0) = 0 \end{aligned} \tag{3a}$$

If $n = \pm 1$,

$$\begin{aligned} F(0) \pm iG(0) &= 0 \\ \frac{dF}{dr}(0) &= 0 \\ H(0) = T(0) &= 0 \end{aligned} \tag{3b}$$

If $|n| > 1$,

$$\begin{aligned} F(0) = G(0) &= 0 \\ H(0) = T(0) &= 0 \end{aligned} \tag{3c}$$

The governing equations, given in the Appendix, along with relations (2) and (3) constitute a generalized eigenvalue problem and is solved numerically. For a temporal solution (which is intended here), α is real and $\omega = \omega_r + i\omega_i$. Depending on the sign of ω_i, the perturbations are either growing or decaying in time.

The governing equations are discretized using a staggered Chebyshev spectral collocation technique. The method has proven to be robust and very efficient.[7–9] The value of r_{max}, the nondimensional radial position where outer boundary conditions are applied, was varied between 50 and 200. Computations revealed that for r_{max} greater than 80, the results are virtually independent of the truncated domain. Therefore, the far-field boundary conditions are enforced at $r_{max} = 100$.

The resulting discretized system is arranged in the form

$$Dy = \omega Ey \tag{4}$$

D and E, the coefficient matrices, are of the $O(5N)$ where N is the number of Chebyshev polynomials employed. The eigenvector y is represented as

$$y = \begin{Bmatrix} F \\ G \\ H \\ P \\ T \end{Bmatrix} \tag{5}$$

The eigenvalue ω is then obtained using IMSL QZ routine. Throughout this study, the number of polynomials was in the range $80 \leq N \leq 100$ to ensure five or six significant figure accuracy.

III. Mean Flowfield

The velocity profile employed in this study is the similarity solution for an axisymmetric incompressible jet with weak swirl obtained by Görtler[10] and independently by Loitsyanskii.[11] For axisymmetric nonswirling compressible jets, Krzywoblocki[12] found the velocity profile does not deviate significantly from the incompressible case up to low supersonic Mach numbers. Therefore, it is assumed here that the addition of weak swirl does not alter the conclusion of Krzywoblocki[12] and the velocity profile obtained by Görtler[10] can be employed in a compressible regime.

Görtler's[10] zeroth-order solution of a swirling jet is as follows:

Mean radial velocity

$$U^* = \frac{K\nu}{z} \frac{2\left[(r^*/r_0) - \left(r^{*3}/r_0^3\right)\right]}{\left[1 + \left(r^{*2}/r_0^2\right)\right]^2} \tag{6a}$$

Mean azimuthal velocity

$$V^* = \frac{C_1 z_0^2}{z^2} \frac{2r^*/r_0}{\left[1 + \left(r^{*2}/r_0^2\right)\right]^2} \tag{6b}$$

Mean axial velocity

$$W^* = \frac{K^2\nu}{z} \frac{2}{\left[1 + \left(r^{*2}/r_0^2\right)\right]^2} \tag{6c}$$

where the $*$ denotes the dimensional quantity, K is proportional to the streamwise momentum flux $2\pi \int_0^\infty \rho^* W^{*2} r^* \, dr^*$, and z_0 is an arbitrary location at which the initial swirl distribution is specified. C_1 is a constant which according to Görtler[10] is obtained from the specified swirl distribution at z_0 regardless of the strength or weakness of the distribution. On the other hand, Loitsyanskii[11] obtained C_1 from the principal moment of momentum with respect to the jet axis. However, it can be shown that the two definitions are interrelated. The length scale $r_0 = z \tan \phi_0$ is a measure of jet spread, and

$\phi_0 \approx \tan^{-1} 2/K$ is the spreading angle for K large (ϕ_0 small). Following Batchelor and Gill[13] and Lessen and Singh,[14] the velocities are normalized with the maximum axial velocity, given by

$$W_0 = 2K^2\nu/z \tag{7}$$

The swirling jet velocity profiles then become

$$U = \frac{1}{K}\frac{(r - r^3)}{(1+r^2)^2}$$

$$V = \frac{C_1 z_0^2}{K^2 \nu z}\frac{r}{(1+r^2)^2} \tag{8}$$

$$W = 1/(1+r^2)^2$$

The flow Reynolds number is then $W_0 r_0/\nu = 4K$ for large K.

Flows of practical interest have very high Reynolds numbers, for which it can be shown[13,14] that $U/W \ll 1$. Furthermore, the characteristic quantities r_0 and W_0 do not change significantly over one wavelength of the disturbances. Therefore, the flow is assumed to be locally parallel, which results in

$$U \approx 0 \tag{9}$$

Moreover, the azimuthal velocity is written as

$$V = \sigma r/(1+r^2)^2 \tag{10}$$

where $\sigma = C_1 z_0^2/K^2\nu z$ can be viewed as a measure of mean flow angularity. However, for incompressible flows it is known[15] that the stability of swirling flows is dependent on the swirl ratio q. Since maximum axial velocity is unity, the swirl ratio then is a measure of the amount of rotation imparted to the jet as a percentage of axial flow. For the profile given by Eq. (10), q is related to σ via

$$q = 0.32475\sigma \tag{11}$$

In regard to the similarity solution (6) or (8) and (10) several important points need to be emphasized. First, owing to the three dimensionality and curvature effects of the mean flow, no transformation of the Dorodnitsyn–Howarth type[16] can be devised to obtain the compressible counterpart of Eq. (6). Second, although Mayer and Powell[17] have recently obtained a similarity solution for a certain class of compressible leading-edge vortices, these solutions are quite dissimilar to the swirling jet profile employed in this study. Most notably, from Eq. (10) the circulation for the rotating jet (which is a measure of the angular momentum present) is given by

$$\Gamma = rV = \sigma r^2/(1+r^2)^2$$

At the far field, the circulation behaves like

$$\Gamma \sim 1/r^2$$

which shows the angular momentum is finite and at the same time Γ is not a monotonic function of the radial coordinate. In contrast, a single isolated line vortex has an infinite angular momentum, and Γ is a monotonic function of r. Thus, we suspect a free vortex and a rotating jet have different stability characteristics. The predominant reason for choosing profile (6) as opposed to a vortex was that profile (6) was a better match to the experimentally measured profiles of Taghavi et al.[4] and Panda and McLaughlin.[18] Although, as remarked at the beginning of this section, for low to moderate Mach numbers, the compressibility effect on the mean velocity profile is assumed to be negligible. The previously presented assumption eventually must be substantiated experimentally.

Returning to Eq. (10), for sufficiently weak swirl ($q < 0.1$ or when $V_{\max}$ is an order of magnitude less than $W_{\max}$), the mean flow has a negligible radial pressure gradient. That is,

$$\frac{\partial \Pi}{\partial r} \approx 0 \tag{12}$$

This condition is an essential requirement both to justify utilizing the mean flow given by Eqs. (8) and to determine the radial temperature distribution (shown subsequently).

For such weak swirl, temperature is assumed to be function of axial velocity only. Taking $Pr = 1$, the radial profile of temperature is obtained via Crocco's relation. It should be emphasized here that the case of $Pr = 1$ is a special one, and in reality the thermodynamic variables could be strongly dependent on the Prandtl number[19] which in turn may alter the disturbance's growth rate. Unfortunately, our understanding of this dependency for three-dimensional swirling flows is totally lacking and, therefore, we restrict ourselves to this special case in the present study. The temperature profile is given by

$$\eta(r) = \beta + (1-\beta)W + (\gamma - 1)M^2[W(1-W)/2] \tag{13}$$

with

$$\beta = \eta_\infty/\eta_0$$

where η_0 is the centerline temperature. Throughout this study, β is taken to be one since computations showed the results to be almost independent of this parameter for $0.7 < \beta < 1.3$. Utilizing Eq. (13) the mean density is then obtained via

$$\rho(r) = 1/\eta(r) \tag{14}$$

From Eq. (13) and for $\beta \approx 1$ some bound on the variation of mean temperature and density across the jet can be given. The temperature scales with M^2 and may be represented as

$$\eta(r) \approx 1 + \frac{(\gamma - 1)}{2}M^2 g(W)$$

where the function

$$g(W) = W - W^2$$

This function has a maximum at $W = 0.5$ with

$$g(0.5) = 0.25$$

Thus,

$$\eta_{\max} \approx 1 + 0.05M^2$$

which indicates for $M \leq 1.4$ the temperature and, hence, density variations are less than 10%.

IV. Results and Discussions

Although the code is written for a flow with variable properties, for the range of Mach number considered in this study (M = 0–1.4) constant properties and $\lambda = -2/3\mu$ are assumed. Even though supersonic combustors operate at much higher M, the present study made a conscious choice to isolate the effects of compressibility on rotation and to not be concerned about the additional variables (κ, μ, etc.). The case of higher Mach numbers (and variable properties) is left for a follow-on study. As a test case (to validate the code), in the limit of $M \approx 0$ and $q = 0$, the stability of an incompressible nonswirling axisymmetric jet was considered. These computations produced identical results to those presented by Lessen and Singh.[14]

Owing to the multidimensional parameter space involved (Re, M, q, α, etc.), for the problem to be tractable, some restriction on the values of these parameters is warranted. As explained earlier, q is confined to <0.1 and $0 \leq M \leq 1.4$. The swirl ratios in this study are selected to be close to the experimental value extracted from the fully developed profile of Taghavi et al.[4] Furthermore, since jet instabilities are inviscid in nature and preliminary results indicated that for $Re > 900$ the growth rate of disturbances approach their inviscid values very rapidly, most of the computations presented in this work are for $Re = 10^3$.

The mean velocity profile employed in the present study is shown in Fig. 1 for a swirl ratio $q = 0.04$. It is well known[13,14] that a fully developed axisymmetric nonrotating jet is only unstable to three-dimensional disturbances having azimuthal wave numbers $n = \pm 1$.

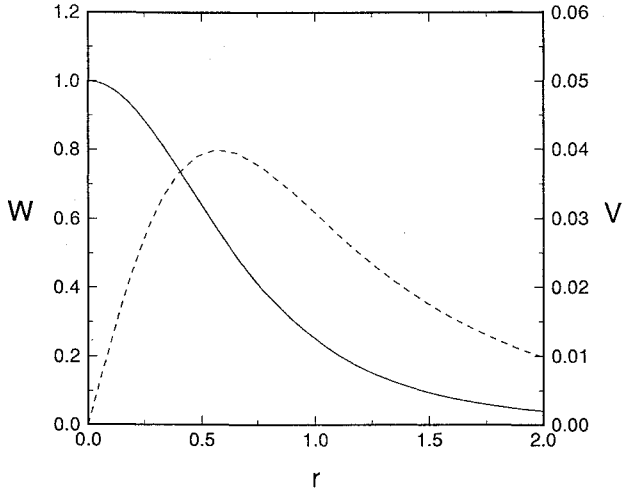

Fig. 1 Mean velocity profile for an axisymmetric rotating jet; —, W and - - - -, V.

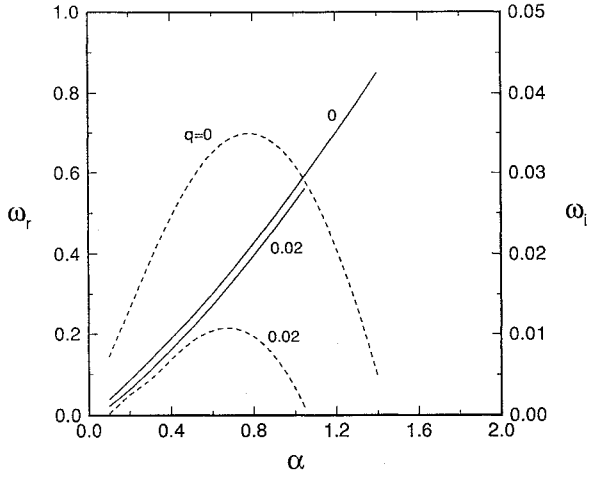

Fig. 2 Effect of adding swirl on the $n = 1$ instability with $M = 0$ and $Re = 10^3$; —, ω_r and - - - -, ω_i.

Figure 2 shows the effect of introducing swirl on the $n = 1$ modes for $M \approx 0$ and $Re = 10^3$. With the addition of only 2% swirl ($q = 0.02$), the growth rate of disturbance ω_i is greatly diminished. Increasing the swirl further stabilized the flow and resulted in a fully damped mode. Thus, the addition of swirl stabilizes the disturbances with positive azimuthal wave number, in agreement with Coleman.[6] However, the situation for $n < 0$ modes proved to be quite different. The variation of the growth rate of the $n = -1$ mode with axial wave number for $q = 0$, $Re = 10^3$, and three different Mach numbers is shown in Fig. 3. The significant damping effect of higher Mach numbers (as reported by many previous investigators) is clearly demonstrated in this figure. Note the maximum ω_i for the $M \approx 0$ curve since it will be the reference value for comparing the growth rates associated with the rotating jets.

Figure 4 displays the effect of adding 4% swirl ($q = 0.04$) on the $n = -1$ disturbances for identical conditions to the previous figure. The growth rate curves show a three- to six-fold increase over the no-swirl results shown in Fig. 3. At the same time, there is a broadening of the region of instability in the axial wave number space (α). The general damping trend of higher M is also present for a swirling jet, whereas the effect on the axial phase speed of disturbances ω_r/α is negligible. However, it is clear that rotation tends to decrease the percentage of drop in the maximum value of ω_i due to the increase in Mach number. Figure 5 displays the effect of increasing swirl on the $n = -1$ mode for $\alpha = 0.8$, $M = 0.8$, and $Re = 10^3$. From this figure, as an example, it was determined that with the addition of only 4% swirl, the growth rate of the $n = -1$ disturbances is increased by more than 300%. Also note the presence

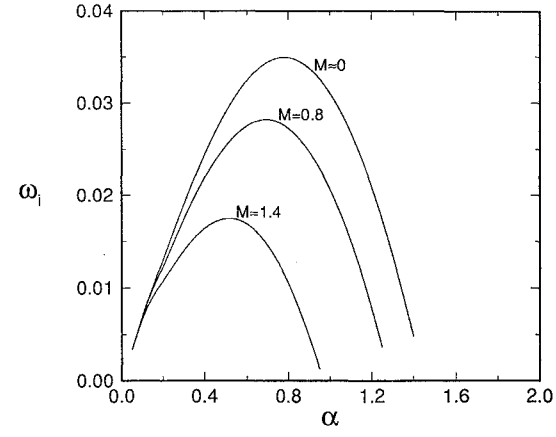

Fig. 3 Effect of Mach number on the growth rate of $n = -1$ disturbances for a nonrotating jet ($q = 0$) with $Re = 10^3$.

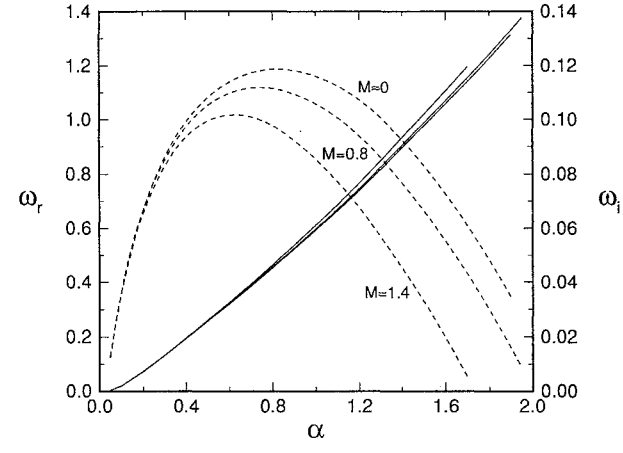

Fig. 4 Effect of Mach number on the $n = -1$ disturbances for a swirling jet ($q = 0.04$) with $Re = 10^3$; —, ω_r and - - - -, ω_i.

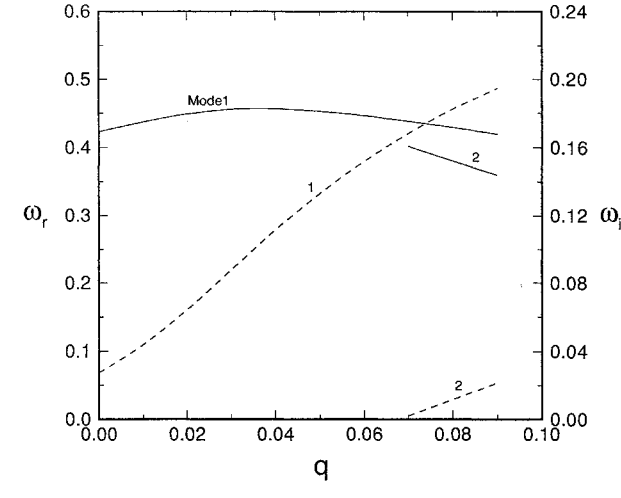

Fig. 5 Effect of increasing swirl ratio on the $n = -1$ perturbations with $\alpha = 0.8$, $M = 0.8$, and $Re = 10^3$; —, ω_r and - - - -, ω_i.

of a second mode of instability as q is increased beyond 0.07. This is an expected behavior for swirling flows.[15] The computations were stopped at $q = 0.09$ since, for larger swirl, the validity of the mean flowfield employed becomes increasingly questionable. The influence of Reynolds number on the asymmetric $n = -1$ mode is shown in Fig. 6 for $\alpha = 0.7$, $q = 0.04$, and $M = 0.8$. As the Reynolds number is increased, ω_i increases and rapidly asymptotes to its inviscid value. The effect of Mach number on this mode for $\alpha = 0.8$, $q = 0.04$, and $Re = 10^3$ is presented in Fig. 7. As mentioned earlier, for moderate values of M, the reduction in the growth rate is slight.

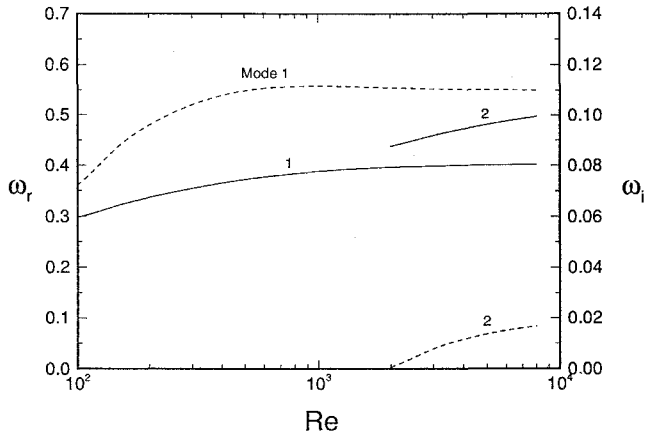

Fig. 6 Influence of Reynolds number on $n = -1$ disturbances with $\alpha = 0.7$, $q = 0.04$, and $M = 0.8$; —, ω_r and - - - -, ω_i.

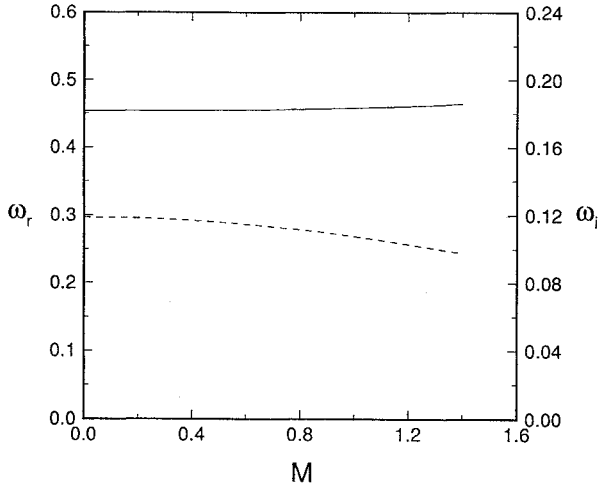

Fig. 7 Variation of the frequency vs Mach number for $n = -1$ disturbances with $\alpha = 0.8$, $q = 0.04$, and $Re = 10^3$; —, ω_r and - - - -, ω_i.

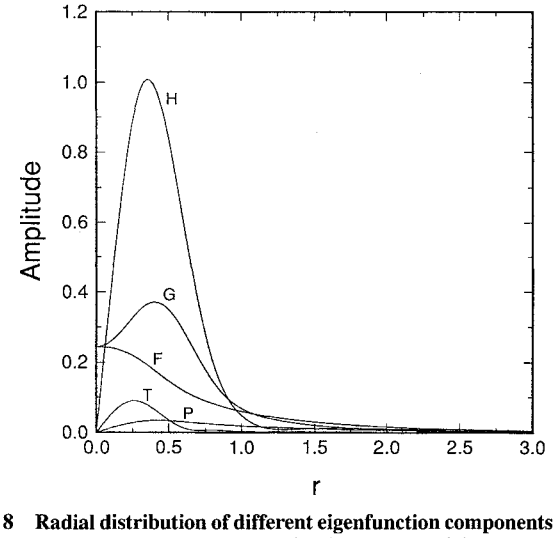

Fig. 8 Radial distribution of different eigenfunction components associated with $n = -1$ mode for a rotating jet with $\alpha = 0.8$, $q = 0.04$, $M = 0.8$, and $Re = 10^3$.

A better understanding of the structure of $n = -1$ mode is gained by examining the eigenfunctions. Remember that F, G, and H are the radial, azimuthal, and axial component of velocity perturbation whereas T and P represent temperature and pressure. The radial distribution of amplitude of different components of $n = -1$ eigenfunction (for identical conditions as in previous figure) is presented in Fig. 8. The amplitudes are normalized by $H_{\max}$. The curves indicate that most of the energy associated with the $n = -1$ mode is concentrated off the centerline at nondimensional radius $r \approx 0.35$. The shape of the eigenfunctions did not change significantly with Mach number except for magnitude of $T_{\max}$ which became larger as M was increased.

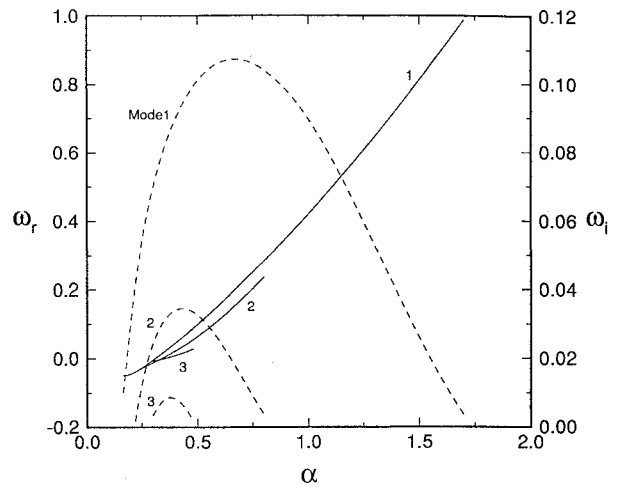

Fig. 9 Variation of the frequency vs axial wave number for $n = -2$ disturbances with $q = 0.06$, $M = 0.8$, and $Re = 10^3$; —, ω_r and - - - -, ω_i.

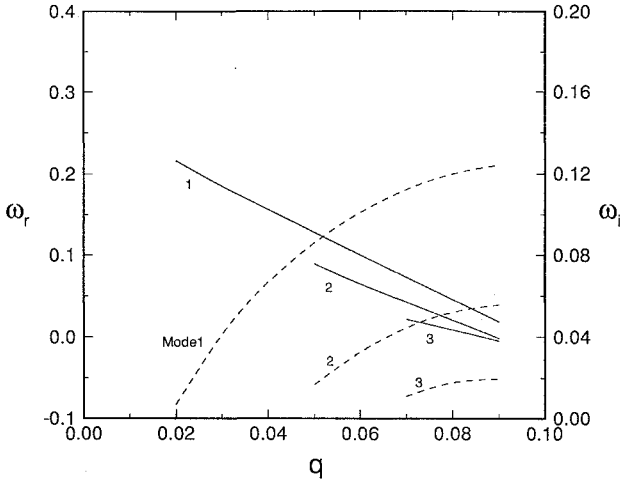

Fig. 10 Effect of increasing swirl ratio on the $n = -2$ perturbations with $\alpha = 0.5$, $M = 0.8$, and $Re = 10^3$; —, ω_r and - - - -, ω_i.

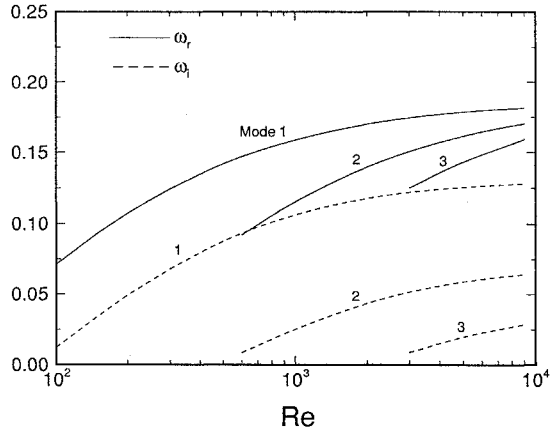

Fig. 11 Influence of Reynolds number on $n = -2$ perturbations with $\alpha = 0.6$, $q = 0.06$, and $M = 0.8$.

The variation of complex frequency ω with α for $n = -2$ modes is presented in Fig. 9. The computations were performed for $q = 0.06$, $M = 0.8$, and $Re = 10^3$. Recall that a fully developed nonswirling axisymmetric jet is stable to such disturbances or any other modes with higher azimuthal wave numbers. Figure 9

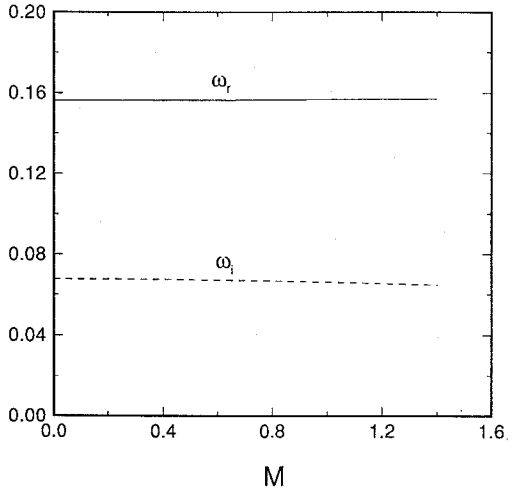

Fig. 12 Variation of the frequency vs Mach number for $n = -2$ disturbances with $\alpha = 0.5$, $q = 0.04$, and $Re = 10^3$.

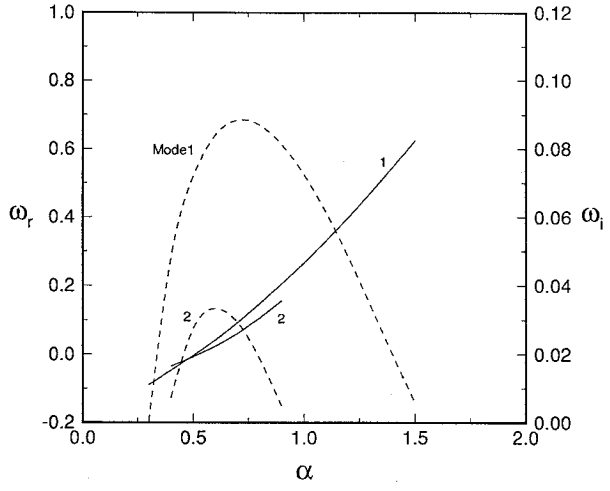

Fig. 13 Variation of the frequency vs axial wave number for $n = -3$ disturbances with $q = 0.06$, $M = 0.8$, and $Re = 10^3$; —, ω_r and - - - -, ω_i.

depicts an instability with comparable growth rate to the $n = -1$ modes (Fig. 4). Similarly, there are higher modes present. The effect of higher swirl on this mode for $\alpha = 0.5$, $M = 0.8$, and $Re = 10^3$ is displayed in Fig. 10. The destabilizing influence of swirl is clearly seen in the increasing growth rates of the perturbations. The influence of Reynolds number on $n = -2$ perturbations is shown in Fig. 11. Unlike the asymmetric mode, the growth rate requires considerably larger Re to acquire its inviscid value. The effect of Mach number on $n = -2$ modes is shown in Fig. 12 for $\alpha = 0.5$, $q = 0.04$, and $Re = 10^3$. For the range of M considered, the stabilizing effect due to compressibility is almost nonexistent for this disturbance.

The results for $n = -3$ perturbations are displayed in Figs. 13–15 which show a nearly identical behavior to the $n = -2$ modes. The variation of the first five azimuthal wave numbers with α at $Re = 10^3$, $M = 0.8$, and $q = 0.06$ is shown in Fig. 16. Notice the severe damping effect of viscosity on the large $|n|$ modes. Obviously, at low Reynolds numbers, the jet downstream development is very much dominated by the $n = -1$ disturbances. At a $Re = 10^4$ (Fig. 17), although the $n = -1$ mode remains unchanged, there is a significant increase in the growth rate of higher modes. Thus at moderate and large Reynolds numbers, the jet development is very much affected by the higher n modes. Furthermore, from Figs. 16 and 17 as Re is increased the range of α where the $n = -2$ mode is unstable shrinks. This means that viscosity has both a stabilizing and destabilizing influence on these inviscid disturbances. Computations revealed that further increasing Re does not result in a significantly higher peak growth rate for the modes shown in Fig. 17. Finally, the $n = -5$ eigenfunctions corresponding to $\alpha = 1.0$, $Re = 10^4$, $M = 0.8$, and $q = 0.06$ are displayed in Fig. 18.

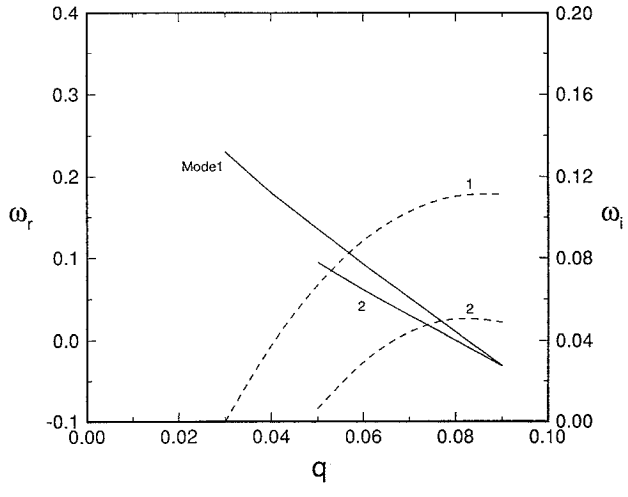

Fig. 14 Effect of increasing swirl ratio on the $n = -3$ perturbations with $\alpha = 0.7$, $M = 0.8$, and $Re = 10^3$; —, ω_r and - - - -, ω_i.

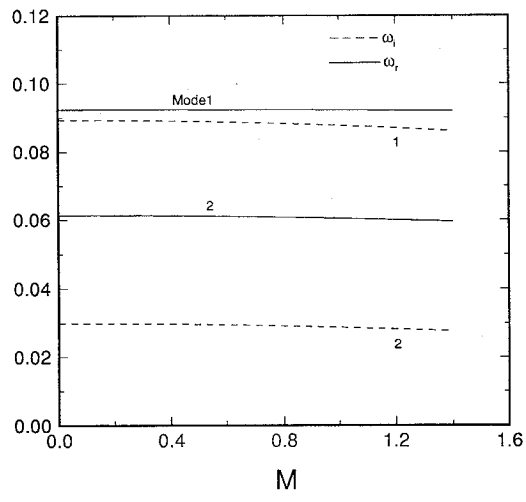

Fig. 15 Variation of the frequency vs Mach number for $n = -3$ disturbances with $\alpha = 0.7$, $q = 0.06$, and $Re = 10^3$.

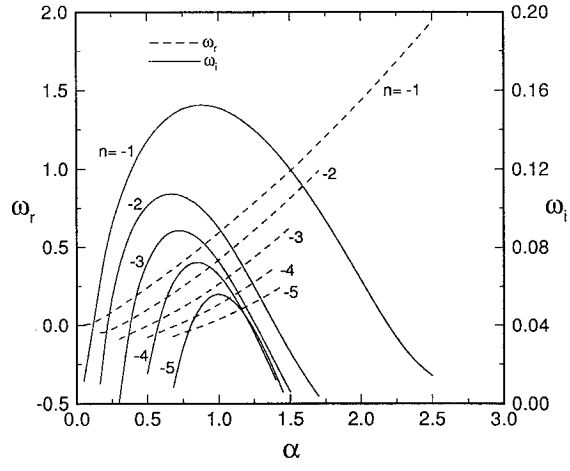

Fig. 16 Variation of ω vs α for the first five negative azimuthal wave number with $q = 0.06$, $M = 0.8$, and $Re = 10^3$.

The eigenfunctions are concentrated off the jet centerline at $r \approx 0.5$. Based on the eigenfunction distribution, the question arises as to whether these unstable disturbances are ring modes. To answer the question, let

$$\Lambda(r) = \alpha W + n(V/r) - \omega \tag{15}$$

then according to the inviscid, incompressible analysis of Leibovich and Stewartson[20] and Duck,[21] for large $|n|$, the criterion for the

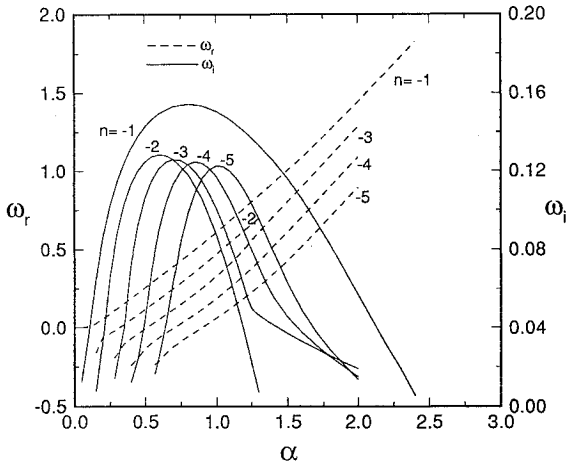

Fig. 17 Variation of ω vs α for the first five negative azimuthal wave number with $q = 0.06$, $M = 0.8$, and $Re = 10^4$.

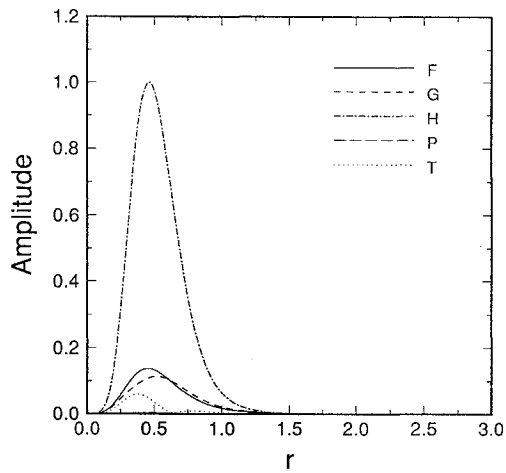

Fig. 18 Radial distribution of different eigenfunction component associated with $n = -5$ mode for a rotating jet with $\alpha = 1.0$, $q = 0.06$, $M = 0.8$, and $Re = 10^4$.

existence of ring modes is given by

$$\frac{d\Lambda}{dr} = 0 = \alpha\frac{dW}{dr} + n\frac{d}{dr}\left(\frac{V}{r}\right) \tag{16}$$

which presumably must be satisfied at some radial position r_c. At a first glance, the Eq. (16) condition cannot be satisfied by the mean velocity profile employed in this study except at $r = 0$ and $r = \infty$ which are irrelevant. However, notice that from Eqs. (8) and (10)

$$V/r = \sigma W$$

and, therefore, Eq. (16) can be rewritten as

$$(\alpha + \sigma n)\frac{dW}{dr} = 0 \tag{17}$$

Interestingly, this condition is met for all values of r if

$$\alpha + \sigma n = 0 \qquad \text{or} \qquad \alpha/n = -\sigma \tag{18}$$

and $n < 0$, even though there is no critical layer in the flowfield. Relation (18) also represents the principal zero strain rate direction. For large azimuthal wave numbers, this is the direction which rotating flows could accommodate unstable waves.[20] Alternatively, one may try to determine r_c from the critical layer condition

$$\Lambda_r = \alpha W + n(V/r) - \omega_r = 0 \tag{19}$$

where subscript r denotes the real part. For the present case, rearranging Eq. (19) in the form

$$(\alpha + \sigma n)W - \omega_r = 0 \tag{20}$$

Table 1 Variation of scaled wave number $|\alpha/n|$ with azimuthal wave number, flow parameters are identical to those specified in Fig. 17

n	α^n	$\lvert\alpha/n\rvert^a = \sigma$	α^b	$\lvert\alpha/n\rvert^b$	α^c	$\lvert\alpha/n\rvert^c$
−1	0.1848	0.1848	0.05	0.05	0.8	0.8
−2	0.3695	0.1848	0.32	0.16	0.6	0.3
−3	0.5543	0.1848	0.51	0.17	0.71	0.2367
−4	0.7390	0.1848	0.70	0.175	0.85	0.2125
−5	0.9238	0.1848	0.89	0.178	1.01	0.202
-10^d	1.848	0.1848	1.835	0.1835	1.885	0.1885

[a]Corresponds to the inviscid criterion (18) with $\sigma = 0.1848$.
[b]Corresponds to the location of $\omega_r = 0$ in Fig. 17.
[c]Corresponds to the location of $\omega_{i_{max}}$ in Fig. 17.
[d]These computations were not presented in Fig. 17.

it becomes clear that depending on the values of α, n, and ω_r there may exist an r_c where relation (20) is satisfied. For the specific case of Eq. (18) one must then concurrently have

$$\omega_r = 0 \tag{21}$$

which once again does not reveal any information regarding r_c. Based on the computed results (Fig. 17), it was determined that for the unstable modes, both conditions (18) and (21) were satisfied. The results are tabulated in Table 1 which shows a comparison between different values of axial wave number corresponding to the theoretical criterion (18), $\omega_r = 0$, and $\omega_{i_{max}}$. Note that as $|n|$ is increased the scaled wave numbers $|\alpha/n|$ corresponding to $\omega_r = 0$ and $\omega_{i_{max}}$ approach the theoretical value σ from below and above, respectively, even though the compressibility effects were completely ignored. Although Table 1 proves the usefulness of condition (18), it nevertheless remains unclear at this time as to whether these unstable modes can be termed ring modes.

The disappearance of Mach number effect for $n < -1$ modes is a puzzling behavior which is contrary to the trends obtained for disturbances of two-dimensional as well as axisymmetric free shear layers. Although addition of swirl does show promise for mixing enhancement, more extensive studies are needed to fully understand the effect of rotation on the stability characteristics of a compressible shear layer.

The present study is incomplete in two respects. First, the fully developed mean flow employed precludes analysis of axisymmetric disturbances in a rotating jet. Such disturbances are an integral part of jet development in its initial stages. Therefore, the stability of near-field profiles needs to be considered. Second, the neglected nonparallel effect may play an important role in jet instability. Both of these areas are currently under investigation and will be reported in the future.

V. Conclusions

Temporal linear stability of a compressible swirling axisymmetric jet was considered. The analysis is valid for weak swirl and parallel mean flow. For the range of Mach number ($0 \lesssim M \leq 1.4$) considered, the flow is assumed to have constant properties. Based on the numerical computations, the following conclusions can be drawn.

1) In the linear regime, the growth rate of $n = -1$ disturbances is substantially increased with the addition of swirl.

2) Disturbances with higher negative azimuthal wave numbers than $n = -1$ become highly unstable. Such perturbations are stable for a fully developed nonswirling jet.

3) The stabilizing influence of higher Mach numbers is greatly diminished with the introduction of swirl to the jet flow.

Appendix

Continuity:

$$\frac{dF}{dr} + \left[\frac{1}{\Pi}\frac{d\Pi}{dr} - \frac{1}{\eta}\frac{d\eta}{dr} + \frac{1}{r}\right]F + \left[\frac{in}{r}\right]G + [i\alpha]H$$

$$+ \left[\frac{U}{\Pi}\right]\frac{dP}{dr} + \left[\frac{1}{\Pi}\frac{d\Pi}{dr} - \frac{1}{\eta}\frac{d\eta}{dr} + \frac{1}{r}\right]F + \left[\frac{in}{r}\right]G$$

$$+[i\alpha]H+\left[\frac{U}{\Pi}\right]\frac{dP}{dr}-\left[\frac{U}{\eta}\right]\frac{dT}{dr}+\left[\frac{2U}{\eta^2}\frac{d\eta}{dr}-\frac{U}{\Pi\eta}\frac{d\Pi}{dr}\right.$$
$$\left.-\frac{inV}{r\eta}-\frac{1}{\eta}\left(\frac{dU}{dr}+\frac{U}{r}\right)-\frac{i\alpha W}{\eta}+\frac{i\omega}{\eta}\right]T=0$$

r momentum:

$$\left[2+\frac{\lambda}{\mu}\right]\frac{d^2F}{dr^2}+\left[-\frac{Re\rho U}{\mu}+\frac{1}{\mu}\frac{d\eta}{dr}\left(2\frac{d\mu}{d\eta}+\frac{d\lambda}{d\eta}\right)\right.$$
$$+\frac{1}{r}\left(2+\frac{\lambda}{\mu}\right)\Bigg]\frac{dF}{dr}+\left[\frac{i\omega Re\rho}{\mu}-\frac{Re\rho}{\mu}\frac{dU}{dr}-\frac{inRe\rho V}{\mu r}\right.$$
$$\left.-\frac{i\alpha Re\rho W}{\mu}+\frac{2}{\mu r}\frac{d\lambda}{d\eta}\frac{d\eta}{dr}-\frac{1}{r^2}\left(2+\frac{\lambda}{\mu}\right)-\frac{n^2}{r^2}-\alpha^2\right]F$$
$$+\left[\frac{in}{r}\left(1+\frac{\lambda}{\mu}\right)\right]\frac{dG}{dr}+\left[\frac{2Re\rho V}{\mu r}+\frac{in}{r\mu}\frac{d\lambda}{d\eta}\frac{d\eta}{dr}\right.$$
$$\left.-\frac{in}{r^2}\left(3+\frac{\lambda}{\mu}\right)\right]G+\left[i\alpha\left(1+\frac{\lambda}{\mu}\right)\right]\frac{dH}{dr}+\left[\frac{i\alpha}{\mu}\frac{d\lambda}{d\eta}\frac{d\eta}{dr}\right]H$$
$$-\left[\frac{Re}{\mu}\right]\frac{dP}{dr}-\left[\frac{Re\rho}{\mu\Pi}\left(U\frac{dU}{dr}-\frac{V^2}{r}\right)\right]P$$
$$+\left[\frac{2}{\mu}\frac{d\mu}{d\eta}\frac{dU}{dr}+\frac{1}{\mu}\frac{d\lambda}{d\eta}\left(\frac{dU}{dr}+\frac{U}{r}\right)\right]\frac{dT}{dr}$$
$$+\left[\frac{2}{\mu}\frac{d^2\mu}{d\eta^2}\frac{d\eta}{dr}\frac{dU}{dr}+\frac{2}{\mu}\frac{d\mu}{d\eta}\frac{d^2U}{dr^2}+\frac{1}{\mu}\frac{d^2\lambda}{d\eta^2}\frac{d\eta}{dr}\left(\frac{dU}{dr}+\frac{U}{r}\right)\right.$$
$$+\frac{1}{\mu}\frac{d\lambda}{d\eta}\left(\frac{d^2U}{dr^2}-\frac{U}{r}+\frac{1}{r}\frac{dU}{dr}\right)+\frac{in}{\mu}\frac{d\mu}{d\eta}\left(\frac{1}{r}\frac{dV}{dr}-\frac{V}{r}\right)$$
$$+\frac{Re\rho}{\mu\eta}\left(U\frac{dU}{dr}-\frac{V^2}{r}\right)+\frac{i\alpha}{\mu}\frac{d\mu}{d\eta}\frac{dW}{dr}$$
$$\left.+\frac{2}{\mu}\frac{d\mu}{d\eta}\left(\frac{1}{r}\frac{dU}{dr}-\frac{U}{r^2}\right)\right]T=0$$

θ momentum:

$$\left[\frac{in}{r}\left(1+\frac{\lambda}{\mu}\right)\right]\frac{dF}{dr}+\left[\frac{in}{r^2}\left(3+\frac{\lambda}{\mu}\right)-\frac{Re\rho}{\mu}\frac{dV}{dr}-\frac{Re\rho V}{\mu r}\right.$$
$$\left.+\frac{in}{r}\frac{1}{\mu}\frac{d\mu}{d\eta}\frac{d\eta}{dr}\right]F+\frac{d^2G}{dr^2}+\left[\frac{1}{\mu}\frac{d\mu}{d\eta}\frac{d\eta}{dr}-\frac{Re\rho U}{\mu}+\frac{1}{r}\right]\frac{dG}{dr}$$
$$+\left[\frac{i\omega Re\rho}{\mu}-\frac{inRe\rho V}{\mu r}-\frac{i\alpha Re\rho W}{\mu}-\frac{Re\rho U}{\mu r}\right.$$
$$\left.-\frac{n^2}{r^2}\left(2+\frac{\lambda}{\mu}\right)-\alpha^2-\frac{1}{r}\frac{1}{\mu}\frac{d\mu}{d\eta}\frac{d\eta}{dr}-\frac{1}{r^2}\right]G$$
$$-\left[\frac{\alpha n}{r}\left(1+\frac{\lambda}{\mu}\right)\right]H-\left[\frac{inRe}{\mu r}+\frac{Re\rho}{\mu\Pi}\left(U\frac{dV}{dr}+\frac{UV}{r}\right)\right]P$$
$$+\left[\frac{1}{\mu}\frac{d\mu}{d\eta}\left(\frac{dV}{dr}-\frac{V}{r}\right)\right]\frac{dT}{dr}+\left[\frac{Re\rho}{\mu\eta}\left(U\frac{dV}{dr}+\frac{UV}{r}\right)\right.$$
$$+\frac{i2nU}{r^2}\frac{1}{\mu}\frac{d\mu}{d\eta}+\frac{in}{\mu}\frac{d\lambda}{d\eta}\left(\frac{1}{r}\frac{dU}{dr}+\frac{U}{r^2}\right)$$
$$+\frac{1}{\mu}\frac{d^2\mu}{d\eta^2}\frac{d\eta}{dr}\left(\frac{dV}{dr}-\frac{V}{r}\right)+\frac{1}{\mu}\frac{d\mu}{d\eta}\left(\frac{d^2V}{dr^2}+\frac{V}{r^2}-\frac{1}{r}\frac{dV}{dr}\right)$$
$$\left.+\frac{2}{r\mu}\frac{d\mu}{d\eta}\left(\frac{dV}{dr}-\frac{V}{r}\right)\right]T=0$$

z momentum:

$$\left[i\alpha\left(1+\frac{\lambda}{\mu}\right)\right]\frac{dF}{dr}+\left[\frac{i\alpha}{r}\left(1+\frac{\lambda}{\mu}\right)-\frac{Re\rho}{\mu}\frac{dW}{dr}+\frac{i\alpha}{\mu}\frac{d\mu}{d\eta}\frac{d\eta}{dr}\right]F$$
$$-\left[\frac{\alpha n}{r}\left(1+\frac{\lambda}{\mu}\right)\right]G+\frac{d^2H}{dr^2}+\left[-\frac{Re\rho U}{\mu}+\frac{1}{\mu}\frac{d\mu}{d\eta}\frac{d\eta}{dr}+\frac{1}{r}\right]\frac{dH}{dr}$$
$$+\left[\frac{i\omega Re\rho}{\mu}-\frac{inRe\rho V}{\mu r}-\frac{i\alpha Re\rho W}{\mu}-\alpha^2\left(2+\frac{\lambda}{\mu}\right)-\frac{n^2}{r^2}\right]H$$
$$-\left[\frac{Re\rho U}{\mu\Pi}\frac{dW}{dr}+\frac{i\alpha Re}{\mu}\right]P+\left[\frac{1}{\mu}\frac{d\mu}{d\eta}\frac{dW}{dr}\right]\frac{dT}{dr}$$
$$+\left[\frac{Re\rho U}{\mu\eta}\frac{dW}{dr}+\frac{i\alpha}{\mu}\frac{d\lambda}{d\eta}\left(\frac{dU}{dr}+\frac{U}{r}\right)\right.$$
$$\left.+\frac{1}{\mu}\frac{d\mu}{d\eta}\left(\frac{d^2W}{dr^2}+\frac{1}{r}\frac{dW}{dr}\right)+\frac{1}{\mu}\frac{d^2\mu}{d\eta^2}\frac{d\eta}{dr}\frac{dW}{dr}\right]T=0$$

Energy equation:

$$\left[2(\gamma-1)M^2Pr\left\{\frac{2\mu}{\kappa}\frac{dU}{dr}+\frac{\lambda}{\kappa}\left(\frac{dU}{dr}+\frac{U}{r}\right)\right\}\right]\frac{dF}{dr}$$
$$+\left[-\frac{PrRe\rho}{\kappa}\frac{d\eta}{dr}+(\gamma-1)M^2Pr\left\{\frac{Re}{\kappa}\frac{d\Pi}{dr}\right.\right.$$
$$+\frac{4\mu}{\kappa}\frac{U}{r^2}+i2\alpha\frac{\mu}{\kappa}\frac{dW}{dr}+\frac{i2n\mu}{r\kappa}\left(\frac{dV}{dr}-\frac{V}{r}\right)$$
$$\left.\left.+\frac{2}{r}\frac{\lambda}{\kappa}\left(\frac{dU}{dr}+\frac{U}{r}\right)\right\}\right]F$$
$$+\left[2(\gamma-1)M^2Pr\frac{\mu}{\kappa}\left(\frac{dV}{dr}-\frac{V}{r}\right)\right]\frac{dG}{dr}$$
$$+\left[\frac{2(\gamma-1)M^2Pr}{r}\left\{\frac{i2n\mu U}{r\kappa}+\frac{in\lambda}{\kappa}\left(\frac{dU}{dr}+\frac{U}{r}\right)\right.\right.$$
$$\left.\left.-\frac{\mu}{\kappa}\left(\frac{dV}{dr}-\frac{V}{r}\right)\right\}\right]G+\left[2(\gamma-1)M^2Pr\frac{\mu}{\kappa}\frac{dW}{dr}\right]\frac{dH}{dr}$$
$$+\left[i2\alpha(\gamma-1)M^2Pr\frac{\lambda}{\kappa}\left(\frac{dU}{dr}+\frac{U}{r}\right)\right]H$$
$$+\left[\frac{(\gamma-1)M^2PrRe}{\kappa}U\right]\frac{dP}{dr}+\left[-\frac{PrRe\rho U}{\kappa\Pi}\frac{d\eta}{dr}\right.$$
$$\left.+\frac{i(\gamma-1)M^2PrRe}{\kappa}\left(-\omega+\frac{nV}{r}+\alpha W\right)\right]P+\frac{d^2T}{dr^2}$$
$$+\left[-\frac{PrRe\rho U}{\kappa}+\frac{2}{\kappa}\frac{d\kappa}{d\eta}\frac{d\eta}{dr}+\frac{1}{r}\right]\frac{dT}{dr}$$
$$+\left[\frac{iPrRe\rho}{\kappa}\left(\omega-\frac{nV}{r}-\alpha W\right)+\frac{PrRe\rho U}{\kappa\eta}\frac{d\eta}{dr}\right.$$
$$+\frac{1}{\kappa}\frac{d^2\kappa}{d\eta^2}\left(\frac{d\eta}{dr}\right)^2-\frac{n^2}{r^2}-\alpha^2+\frac{1}{\kappa}\frac{d\kappa}{d\eta}\left(\frac{d^2\eta}{dr^2}+\frac{1}{r}\frac{d\eta}{dr}\right)$$
$$\left.+(\gamma-1)M^2Pr\frac{1}{\kappa}\frac{d\mu}{d\eta}\left(\frac{dW}{dr}\right)^2\right.$$

$$+\frac{2(\gamma-1)M^2Pr}{\kappa}\frac{d\mu}{d\eta}\left\{\left(\frac{dU}{dr}\right)^2+\frac{U^2}{r^2}\right\}$$

$$+\frac{(\gamma-1)M^2Pr}{\kappa}\frac{d\mu}{d\eta}\left\{\left(\frac{dV}{dr}-\frac{V}{r}\right)^2\right\}$$

$$+\frac{(\gamma-1)M^2Pr}{\kappa}\frac{d\lambda}{d\eta}\left\{\left(\frac{dU}{dr}+\frac{U}{r}\right)^2\right\}\Bigg]T=0$$

Acknowledgment

This work was supported by NASA Langley Research Center (Experimental Flow Physics Branch) under Contract NAS1-18240.

References

[1]Birch, S. F., and Eggers, J. M., "A Critical Review of the Experimental Data for Developed Free Shear Layers," *Free Turbulent Shear Flows*, NASA SP 321, July 1972, pp. 11–40.

[2]Chinzei, N., Masuya, G., Komuro, T., Murakami, A., and Kudou, D., "Spreading of Two-Stream Supersonic Turbulent Mixing Layers," *Physics of Fluids*, Vol. 29, 1986, pp. 1345–1347.

[3]Northam, G. B., private communications, NASA Langley Research Center, May 1990.

[4]Taghavi, R., Rice, E. J., and Farokhi, S., "Large Amplitude Acoustic Excitation of Swirling Turbulent Jets," AIAA Paper 89-0970, March 1989.

[5]Michalke, A., *Survey on Jet Instability Theory*, Progress in Aerospace Sciences, Vol. 21, AIAA, New York, 1984, pp. 159–199.

[6]Coleman, C. S., "The Stability of Swirling Jets," *Astronomical Society of Australia, Proceeding*, Vol. 8, 1989, pp. 38–40.

[7]Macaraeg, M. G., Streett, C. L., and Hussaini, M. Y., "A Spectral Collocation Solution to the Compressible Stability Eigenvalue Problem," NASA Tech. Paper 2858, Dec. 1988.

[8]Khorrami, M. R., Malik, M. R., and Ash, R. L., "Application of Spectral Collocation Techniques to the Stability of Swirling Flows," *Journal of Computational Physics*, Vol. 81, No. 1, 1989, pp. 206–229.

[9]Khorrami, M. R., "A Chebyshev Spectral Collocation Method Using a Staggered Grid for the Stability of Cylindrical Flows," *International Journal for Numerical Methods in Fluids*, Vol. 12, No. 9, 1991, pp. 825–833.

[10]Görtler, H., "Theoretical Investigations of Laminar Boundary Layer, Problem II—Decay of Swirl in an Axially Symmetrical Jet, Far from the Orifice," Air Force Contract No. AF 61 (514)-627-C, March 1954.

[11]Loitsyanskii, L. G., "Propagation of a Rotating Jet in an Infinite Space Surrounded by the Same Liquid," *Prikladnaya Matematika i Mekhanika*, Vol. 17, 1953, pp. 3–16.

[12]Krzywoblocki, M. Z., "On Steady, Laminar, Round Jets in Compressible Viscous Gases far Behind the Mouth," *Osterreichisches Ingenieur Archiv*, Vol. 13, 1949, pp. 373–383.

[13]Batchelor, G. K., and Gill, A. E., "Analysis of the Stability of Axisymmetric Jets," *Journal of Fluid Mechanics*, Vol. 14, 1962, pp. 529–551.

[14]Lessen, M., and Singh, P. J., "The Stability of Axisymmetric Free Shear Layers," *Journal of Fluid Mechanics*, Vol. 60, 1973, pp. 433–457.

[15]Duck, P. W., and Foster, M. R., "The Inviscid Stability of a Trailing Line Vortex," *Journal of Applied Mathematical Physics* (ZAMP), Vol. 31, 1980, pp. 523–530.

[16]Stewartson, K., *The Theory of Laminar Boundary Layers in Compressible Fluids*, Oxford Univ. Press, Oxford, England, UK, 1964, Chap. 2.

[17]Mayer, E. W., and Powell, K. G., "Similarity Solutions for Viscous Vortex Cores," *Journal of Fluid Mechanics*, Vol. 238, 1992, pp. 487–507.

[18]Panda, J., and McLaughlin, D. K., "Experiments on the Instabilities of a Swirling Jet," *Physics of Fluids*, Vol. 6, 1994, pp. 263–276.

[19]Mack, L. M., "The Compressible Viscous Heat-Conducting Vortex," *Journal of Fluid Mechanics*, Vol. 8, 1960, pp. 284–292.

[20]Leibovich, S., and Stewartson, K., "A Sufficient Condition for the Instability of Columnar Vortices," *Journal of Fluid Mechanics*, Vol. 126, 1983, pp. 335–356.

[21]Duck, P. W., "The Inviscid Stability of Swirling Flows: Large Wavenumber Disturbances," *Journal of Applied Mathematics and Physics* (ZAMP), Vol. 37, 1986, pp. 340–360.